

Analyst

Accepted Manuscript

This article can be cited before page numbers have been issued, to do this please use: R. Chen, N. Gumus, S. Jearranaiprepame, A. Woodward, R. Rahman and D. Kim, *Analyst*, 2026, DOI: 10.1039/D5AN00461F.



This is an Accepted Manuscript, which has been through the Royal Society of Chemistry peer review process and has been accepted for publication.

Accepted Manuscripts are published online shortly after acceptance, before technical editing, formatting and proof reading. Using this free service, authors can make their results available to the community, in citable form, before we publish the edited article. We will replace this Accepted Manuscript with the edited and formatted Advance Article as soon as it is available.

You can find more information about Accepted Manuscripts in the [Information for Authors](#).

Please note that technical editing may introduce minor changes to the text and/or graphics, which may alter content. The journal's standard [Terms & Conditions](#) and the [Ethical guidelines](#) still apply. In no event shall the Royal Society of Chemistry be held responsible for any errors or omissions in this Accepted Manuscript or any consequences arising from the use of any information it contains.

ARTICLE

Anti-tumour and associated metabolic effects of repurposed Afuresertib and Taxifolin for glioblastoma treatment

Rui Chen ^a, Nurcan Gumus ^b, Supisara Jearanaipreame ^b, Alison Whitby ^c, Ruman Rahman ^c, and Dong-Hyun Kim ^{*a,d}

Received 00th January 20xx,
Accepted 00th January 20xx

DOI: 10.1039/x0xx00000x

Isocitrate dehydrogenase wild-type glioblastoma (GBM) is a particularly devastating central nervous system tumour with limited treatments. Taking advantage of computational strategies, drug repurposing has been regarded as an alternative and effective tool in GBM drug development, especially models targeting altered metabolic pathways and genomic alterations. In previous work, Afuresertib and Taxifolin were selected as repurposed candidates after the application of Transcriptomics-informed Stoichiometric Modelling and Network analysis. Whilst these two candidates have been studied in the other types of cancers, they have not been tested against GBM. This study explored the *in vitro* anti-tumour effect of Afuresertib and Taxifolin using PrestoBlue metabolic viability assay and Transwell collagen barrier assay on patient-derived glioblastoma cell lines. Their associated metabolic impact was revealed by the application of untargeted metabolomics method. The results showed that Afuresertib had stronger inhibition on GBM cell proliferation and invasion than Taxifolin. Glycerophospholipids metabolism was more active in cells derived from invasion margin relative to cells from tumour core, indicating the possibility of varying underlining genetic mutations between GIN and GCE cell lines. Afuresertib could affect amino acid metabolism and glycerophospholipid metabolism, exerting the function of anti-proliferation and anti-invasion. Taxifolin could damage nicotinate and nicotinamide metabolism, leading to the death of tumour cells.

Introduction

Isocitrate dehydrogenase (IDH) wild-type glioblastoma (GBM) remains a particularly devastating central nervous system tumour with limited treatments¹. Substantial inter- and intra-tumour heterogeneity and a highly invasive nature are regarded as two crucial reasons for minimal progress in effective therapies for GBM². Besides, radio-/chemo-resistance and associated tumour recurrence remain confounding factors for therapy options^{3, 4}. There is therefore an urgent need for the discovery of effective therapies which may be rapidly repurposed for drug development in GBM. Following the identification of IDH wild-type and mutant GBM, increasing evidence has strongly supported the notion that GBM is a metabolic disorder, generating metabolic reprogramming associated with metabolic heterogeneity⁵. Both GBM progression and invasion involve complex interactions

with their metabolic environment^{6, 7}; however, this is not a well understood area. To investigate the alteration in metabolism of GBM, metabolomics is a promising approach with the ability to capture metabolic signatures of a tumour's phenotype⁸. Combined with other omics approaches, several *in vitro* metabolomic studies have been conducted based on both established and primary GBM cell lines, elucidating information regarding altered metabolic pathways and potential biomarkers⁹⁻¹¹. For instance, 2-hydroxyglutarate, glycerophosphocholine, and myo-inositol were reported as highly abundant in IDH mutant GBM¹²⁻¹⁴. These metabolic vulnerabilities of GBM can potentially provide new therapeutic opportunities¹⁵. To translate these metabolic alterations into therapeutic advances, drug repurposing is an increasingly attractive proposition since it employs de-risked compounds (often with established patient safety and toxicological profiles determined for certain indications), providing multiple advantages over discovering and developing an entirely new drug^{16, 17}. Moreover, based on the analysis of large-scale data, computational approaches have primarily been employed in drug repurposing to gain meaningful interpretations for hypotheses generation, particularly through molecular pathway mapping¹⁸. By establishing specific disease networks based on the pathology, genome-wide association studies data or protein/metabolite interactions, network analysis allows identification of highly connected reactions which would potentially disrupt the process of pathophysiology once inhibited¹⁹. In our previous study, a recombinant innovation

^a Centre for Analytical Bioscience, Advanced Materials and Healthcare Technologies Division, School of Pharmacy, University of Nottingham; Nottingham, NG7 2RD, UK
^b Molecular Therapeutics and Formulation Division, School of Pharmacy, University of Nottingham, Nottingham, NG7 2RD, UK
^c Children's Brain Tumour Research Centre, Biodiscovery Institute, School of Medicine, University of Nottingham; Nottingham, NG7 2RD, UK
^d College of Pharmacy, Kyungpook National University, Daegu 41566, Republic of Korea
^e †Electronic Supplementary Information (ESI) available: [details of any supplementary information available should be included here]. See DOI: 10.1039/x0xx00000x

approach was developed, termed 'Transcriptomics-informed Stoichiometric Modelling and Network analysis' (TISMAN). By constructing GBM metabolic models using published transcriptomics datasets, TISMAN identified metabolic reactions of interest prior to screening a chemical-gene interaction database. As a result, five candidates were prioritised: Afuresertib, Taxifolin, Pyrogallol, Isorhamnetin, and Formononetin²⁰.

For evaluating a drug candidate's potential value for GBM therapy, it is reasoned to target the major active pathway in the disease model. The phosphatidylinositol 3-kinase-serine-threonine kinase-mechanistic target of rapamycin (PI3K-AKT-mTOR) pathway has been studied as one of the most frequently altered biochemical signalling cascades in GBM and is related to metabolic regulation of proliferation and migration, thus representing a potential target for drug development and repurposing²¹⁻²³. Among the five selected compounds, combined with literature review, Afuresertib (Figure 1A) and Taxifolin (Figure 1B) have been reported to target the PI3K-AKT-mTOR pathway. Afuresertib, a novel AKT inhibitor, has been demonstrated to reduce the activity of AKT protein within this pathway and has shown potent anti-tumour effects, both preclinically and clinically, across various cancer types including multiple myeloma, leukaemia, oesophageal cancer and ovarian cancer, either as a monotherapy or in combination with other drugs²⁴⁻²⁸. However, its effects have yet to be evaluated on GBM. Taxifolin is a flavonoid, mainly exhibiting antioxidant and anti-inflammatory roles²⁹⁻³¹. Yao *et al* discovered that taxifolin could dually target PI3K and mTOR to inhibit GBM cell growth³². However, it should be noted that the cell lines involved were commercial ones rather than primary patient-derived, and the ability to assess anti-invasion was not taken into consideration. Hence, we hypothesised that Afuresertib and Taxifolin could alter metabolic pathways in GBM to exert an anti-tumour phenotype.

In this study, the anti-tumour effects of repurposed Afuresertib and Taxifolin have been studied on patient derived GBM cell lines and the drug mode of action has been inferred from a metabolomic perspective using liquid chromatography-mass spectrometry (LC-MS)-based metabolite profiling.

Materials and methods

Materials

Afuresertib (Catalog No: S7521, Batch No: 01, Purity: 99.26%) was purchased from Selleck Chemicals LLC (Berlin, Germany). Taxifolin (Catalog No: HY-N0136, Batch No: 23044, Purity: 99.97%) was ordered from MedChemExpress LLC (Monmouth Junction, USA). PrestoBlueTM cell viability reagent (Lot: 2342788), Dulbecco's modified eagle medium (DMEM, Catalog No.: 31885023, Lot No.: 2436216) and 0.5% Trypsin-EDTA (10X) was purchased from Thermo Fisher Scientific Inc. (Leicestershire, UK). Dulbecco's phosphate buffered saline (DPBS), Dimethyl sulfoxide (DMSO) and 0.5% Trypsin-EDTA 10X were ordered from Sigma-Aldrich Co. LLC (Gillingham, UK). Bovine growth serum supplemented calf (FBS) was purchased

from Cytiva (Utah, USA). The phosphate buffered saline (PBS) solution was provided by the laboratory. The kit of astrocyte medium (Lot:34355) and 1 mg/mL poly-L-lysine (PLL, Lot: 33107) were purchased from Caltag Medsystems Ltd. (Buckingham, UK). Cultrex Mouse Collagen IV (Lot: 1578996) was purchased from Bio-Techne Corporation (Minneapolis, USA). 24 well ThinCertTM 8 µm cell culture inserts were ordered from Greiner Bio-One International GmbH (Stonehouse, UK). Cell culture Petri dishes (100×20 mm) were ordered from Corning Incorporated (Flintshire, UK). Ammonium carbonate was purchased from Honeywell International Inc. (Berks, UK). LC-MS grade methanol and acetonitrile were supplied by VWR Chemicals, LLC (Lutterworth, UK). Deionised water was automatically generated from a PURA-Q+ ultrapure water purification system (Scientific Laboratory Supplies, UK).

Cell lines and culture conditions

Glioblastoma invasive margin (GIN28, GIN31) and glioblastoma contrast-enhanced core (GCE28, GCE31) cell lines were previously derived at Queen's Medical Centre from patients undergoing resected tumour surgery. These cell lines were derived from intra-tumour regions of two tumours (patient 28 and patient 31). All cell lines were cultured in antibiotics-free DMEM supplemented with 10% FBS and incubated under humidified growth conditions at 37°C and 5% CO₂.

Cortical astrocytes (healthy counterpart to GBM cells) were purchased from ScienCell Research Laboratories and the process of culture was conducted according to the supplier's instructions.

Metabolic viability assay

5,000 cells/well were seeded in 96-well plates for all patient derived GBM cell lines. After stabilising for 24 h, culture medium was replaced with 100 µL drug-containing medium and incubated for a further 72 h. Multi-point doses of drug treatment were applied, ranging from 1-200 µM for Afuresertib and 1-2,000 µM for Taxifolin respectively. Appropriate vehicle (0.1% DMSO) and positive cell death controls (10% DMSO) were included. Fluorescence at 544/590 nm was measured on a microplate reader (FLUOstar[®] Omega, BMG labtech) after 1h PrestoBlueTM (1:10) incubation. Viability of drug-treated cells was determined by normalising fluorescence intensity against that of vehicle-only control.

For astrocytes, PLL working solution was prepared by adding 150 µL 1mg/mL PLL in 10mL sterile water. The plates were coated with 43 µL PLL working solution overnight and rinsed with 100 µL DPBS before seeding cells. The seeding density of astrocytes was 1,600 cells/well, and multi-point doses were adopted with 1-50 µM for Afuresertib, 1-500 µM for Taxifolin. Two control groups were also included as above. The process of measurement and data analysis were performed as previously described for GBM cell lines.

Invasion assay

To study the capability of drugs to inhibit GBM cell invasion, the Transwell collagen barrier assay was adopted to investigate the response of single cells to the drug treatment³³. Mouse collagen



IV (15 µg/insert) was added into ThinCert™ 8 µm cell culture inserts and coated inserts were then dried in a sterile environment. Prior to seeding cells, 100 µL of DMEM was added to dried collagen soaking for 1 h.

Digested cells were later suspended in DMEM. 100 µL of drug-containing DMEM was added to the pre-soaked insert followed by adding 100 µL of cell suspension. The seeding densities were 12,000 cells/insert for GIN31 and GCE31, and 14,000 cells/insert for GIN28 and GCE28. The bottom chamber was filled with 700 µL of DMEM supplemented with 10% FBS. The plates were incubated for 24 h to allow invasion to commence. For the negative control, inserts contained cells suspended in DMEM supplemented with 10% FBS, while the bottom chamber was filled with DMEM.

When the incubation period concluded, cells were fixed with 700 µL of ice-cold methanol for 1 h after medium was removed. Non-invaded cells were next removed using cotton buds, before inserts being stained in 600 µL of 0.2% crystal violet for 15 min whilst protecting from light. Inserts were washed in water to remove residual dyes and dried overnight. Finally, cells were imaged at four different fields of view under the multi-viewing microscope (Brunel, N-510).

Metabolomics study

Sample preparation

Cells were seeded in Petri dishes and cultured in DMEM supplemented with 10% FBS to harvest 1×10^6 cells at the end of experiments. After 24 h, cells were treated with Afuresetib or Taxifolin followed by 72 h incubation.

To extract intracellular metabolites, cells were quickly washed with pre-warmed PBS twice after removing the medium. Then, 1.0 mL of pre-cooled (-40 °C) methanol was added into each dish followed by rapidly quenching and scraping the cells. Cell suspensions were collected and vortexed for 1 h at 4 °C. Subsequently, the supernatant was collected after centrifugation (13000 rpm/ 5 min) at 4 °C. Next, cell extracts were dried in the vacuum centrifuge evaporator before using 70 µL of LC-MS grade methanol for reconstitution. Last, reconstituted samples were centrifuged again, and the supernatant was transferred to LC-MS vials for analysis.

A pooled quality control (QC) sample was prepared by taking 10 µL aliquots from each sample and mixed into one vial (excluding blank samples) to evaluate the robustness, performance, and stability of the analytical system.

LC-MS-based metabolite profiling

The reagent-blank samples were analysed prior to the experimental samples. Experimental samples were randomised in the sequences with QC samples ($n \geq 6$) analysed intermittently throughout the duration of the analysis. Five mixed authentic standard solutions (total 266 standards) were injected under the same condition for metabolite identification.

Separation was performed on a ZIC-pHILIC column (5 µm, 4.6×150 mm) manufactured by Merck Sequant (Watford, UK) with a guard column, using an Dionex Ultimate 3000 HPLC system (Thermo fisher Scientific, Hemel Hempstead, UK). The

mobile phases consisted of 20 mM ammonium carbonate (A) and acetonitrile (B), using linear gradient (0–15 min: 20% A to 95% A, 15–17 min: 95% A to 20% A, 17–24 min: 20% A). The injection volume was 10 µL and the flow rate was 300 µL/min. The temperature of autosampler and column compartment was maintained at 4 °C and 45 °C respectively.

Detection was conducted on a Q-Exactive Plus hybrid quadrupole-Orbitrap mass spectrometer (Thermo Fisher Scientific, Hemel Hempstead, UK) fitted with HESI source. Data acquisition was performed in rapid polarity-switching mode with spray voltages at +4.5 kV and -3.5 kV, respectively. Other instrument settings were optimised as follows: capillary temperature, 275 °C; sheath gas flow rate, 40; aux gas flow rate, 5; sweep gas flow rate, 1; S-lens RF level, 55%. The samples were acquired at a mass resolution of 70,000 at m/z 200, across an m/z range of 70–1,050 with an automatic gain control (AGC) of 3×10^6 . Top 10 data-dependent MS/MS (ddMS/MS) were performed on QC samples at a mass resolution of 17500 with AGC target 1×10^5 and stepped normalised collision energy of 20, 30 and 40.

Metabolite identification

Total ion chromatograms generated from LC-MS, including experimental samples, QC samples, and blank samples, were displayed and checked using Xcalibur (Thermo Fisher Scientific, Waltham, USA). Raw datasets were subsequently imported into Compound Discover 3.3 SP1 (Thermo Fisher Scientific, Waltham, USA) for peak picking, peak alignment, metabolite identification and gap filling, by applying an untargeted metabolomic workflow with a retention time range between 0.5–23.5 min, peak rating results (>5), and aligned window (within m/z 5 ppm) for precursor and fragment ions. Ions were identified and annotated by matching accurate masses of detected ions with metabolites in the Human Metabolites Database (HMDB)³⁴, the accurate masses and retention times of authentic standards, *mzCloud* fragmentation database and in-house Thermo Scientific *mzVault* spectral libraries.

Ultimately, metabolites were classified into four levels of confidence according to the metabolomics standards initiative and scale^{35, 36}. Level 1 confidence was that the ions matched with the accurate masses, retention times, and fragments of authentic standards. Level 2 confidence represented ions matched to the exact masses and fragments of metabolites in spectral/online libraries in the absence of standards. Level 3 confidence was that ions identification was based only on accurate mass matching with database entries, without supportive fragmentation information. Level 4 confidence referred to ions only with or without predicted molecular formulas.

Pathway analysis and network mapping

In this study, metabolites with level 1 and level 2 identification confidence were applied to the pathway analysis. Pathway analysis was conducted using the online platform of MetaboAnalyst v5.0³⁷. Non-human putative metabolites were excluded.



Statistics

exposure to Afuresertib and Taxifolin are shown in Figure 1C

DOI: 10.1039/D5AN00461F

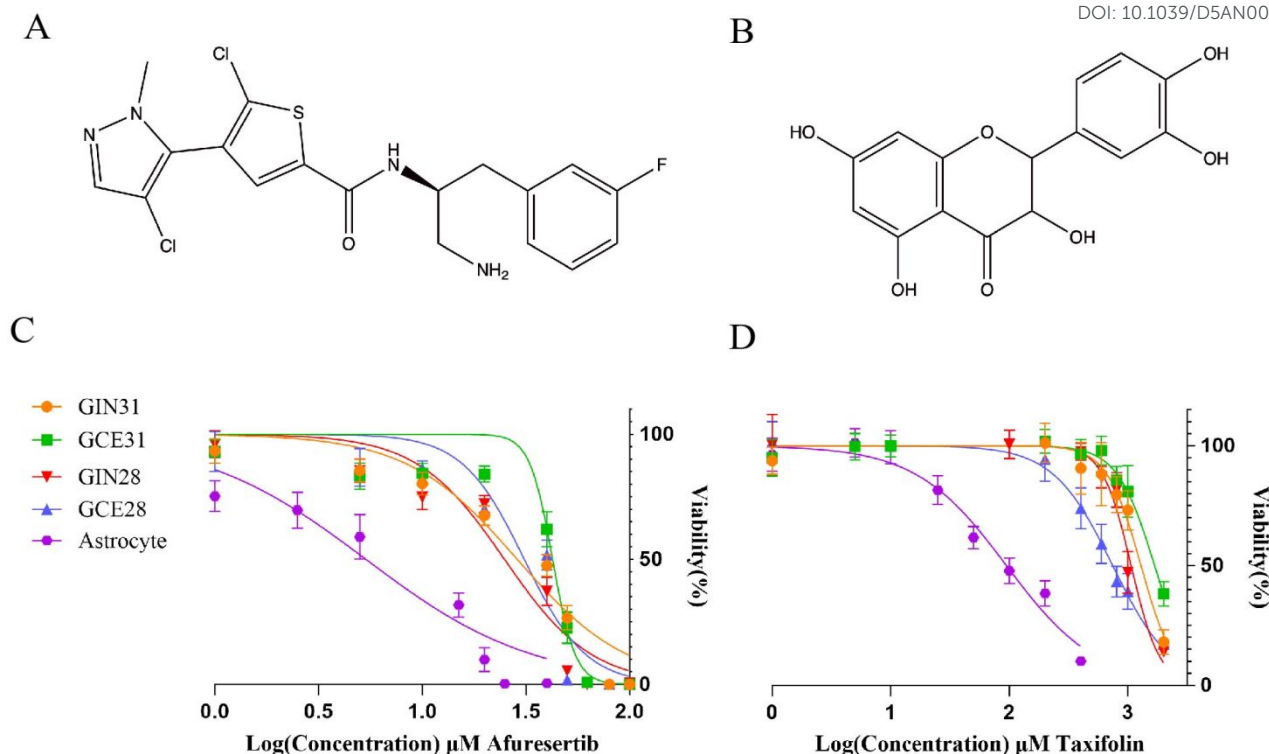


Fig 1. The chemical structure of repurposed drug candidates and assessment of GBM metabolic viability. (A) and (B) are the chemical structure of Afuresertib and Taxifolin. (C) and (D) are the dose-dependent inhibition of GBM cells and astrocytes exposed treatments. The concentration of drug is log10 transformed. The colours and shapes represent distinct cell lines.

For viability and invasion assays, curve fitting of inhibition and statistical data analysis was performed on GraphPad Prism v8.2.1 (GraphPad Software, San Diego, USA). p value <0.05 was considered statistically significant.

For univariate analysis of metabolomics datasets, data was log-transformed. Two-tailed student t -test p value was adjusted using the Benjamini-Hochberg correction for false discovery rate, compensating for the multiple testing problem. Adjusted p value <0.05 was regarded as significant.

Multivariate analysis, including principal component analysis (PCA) and orthogonal partial least squares discriminant analysis (OPLS-DA) was performed on SIMCA-P v16 (Umetrics, Sweden) to determine significant metabolites. After logarithmic transformation, the method of Unit-Variance scaling (UV scaling) and Pareto Scaling (Par scaling) was used for PCA and OPLS-DA respectively.

Results

Metabolic viability

After 72h incubation, metabolic viability was measured using PrestoBlue™, which is a non-toxic, resazurin-based cell health indicator³⁸. Metabolically active cells reduce non-fluorescent resazurin to fluorescent resorufin³⁹. The intensity of fluorescence is relatively linear to the number of living/metabolically active cells. The viability results upon acute

and 1D. The IC_{50} concentration of both compounds against GBM cell lines and astrocytes are summarised in Table 1.

Table 1. The IC_{50} value of Afuresertib and Taxifolin on GBM cells and astrocytes (μM).

Name	Astrocytes	GIN31	GCE31	GIN28	GCE28
Afuresertib	5.353	28.75	42.54	24.95	31.09
Taxifolin	90.20	1287	1676	1067	742.8

Results indicate that both Afuresertib and Taxifolin showed dose-dependent impairment of metabolic viability. Afuresertib was identified as more potent for inhibiting GBM proliferation relative to Taxifolin. Moreover, the cells derived from the invasion margin of GBM (GIN31/28) were more sensitive to Afuresertib than counterpart cells derived from the tumour core (GCE31/28). Astrocytes were also included to explore the selectivity of drug candidates in healthy counterpart cells. The results showed that astrocytes were more sensitive to all candidates than GBM cells, indicating potential toxicity might exist during clinical practice.

LC-MS-based metabolite profiling

After investigating the anti-tumour effects of candidates, LC-MS-based metabolite profiling was employed to explore which metabolites and metabolic pathways were affected or altered by the drug exposure. In order to improve the quality of input data, features were regarded as non-informative and removed

if their relative standard deviations (RSD) were $\geq 30\%$ in the technical replicates of pooled QC samples⁴⁰.

were observed, indicating that these were associated with metabolic alterations resulting from drug exposure.

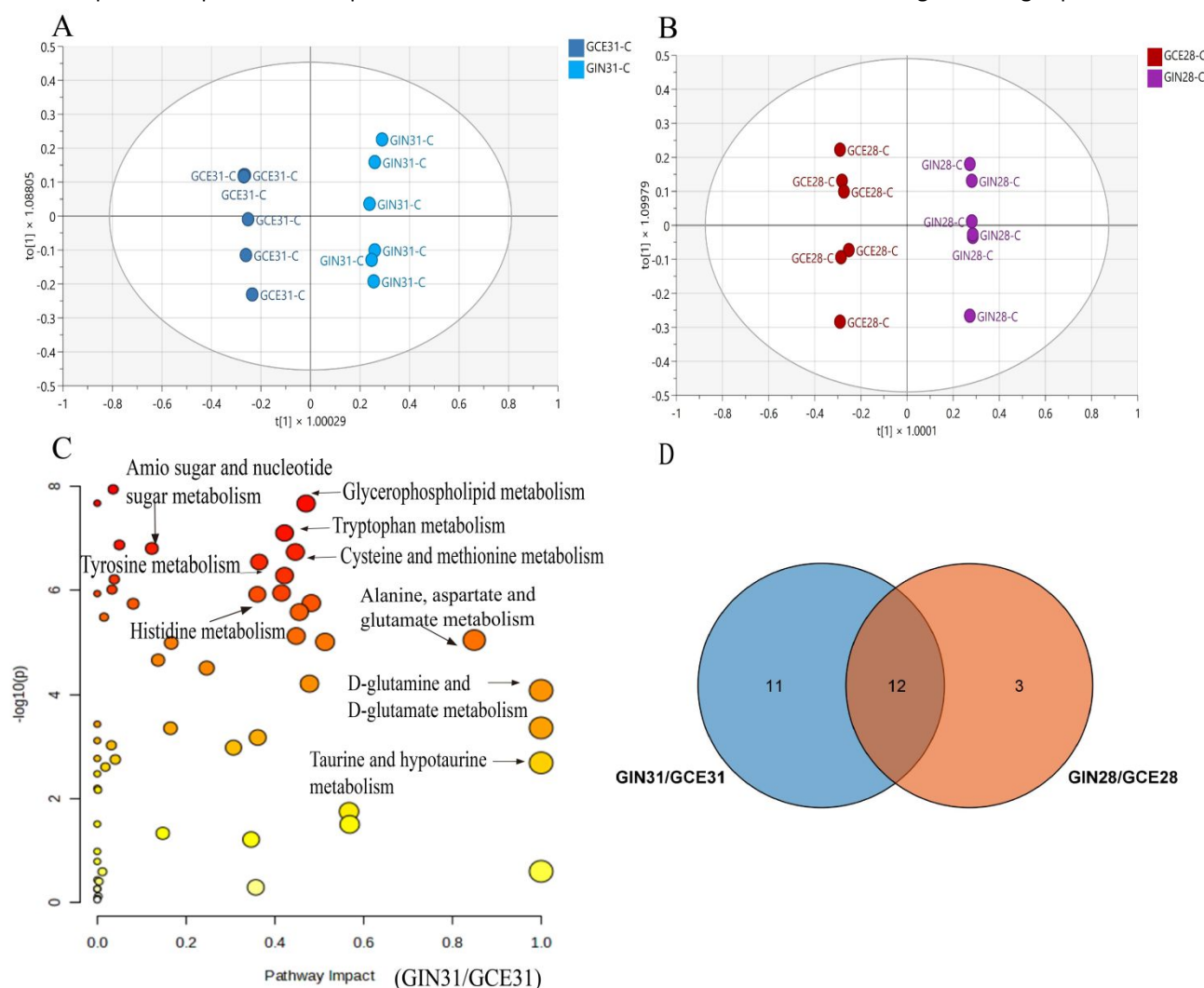


Fig 2. Metabolic variation between GBM cells derived from invasive margin and tumour core. (A) and (B) are the scores plots of constructed OPLS-DA models for GINs/GCEs. The cross-validation results were $R^2Y=0.997$ and $Q^2=0.951$ for GIN31/GCE31, $R^2Y=0.999$ and $Q^2=0.927$ for GIN28/GCE28. (C) is the result of pathway analysis for GIN31/GCE31. The colour (white to red) represents statistical significance. The size of bubble directly related to the number of metabolites mapped on the specific pathway. The pathway impact factor represents the importance of the identified pathway on the whole metabolic network. (D) Venn diagram of the number of identified metabolic pathways when comparing metabolic differences between GINs and GCEs.

For high dimensional datasets, PCA and OPLS-DA are commonly used to construct models that classify samples and distinguish metabolite variations across different experimental conditions. In this study, the information of mass ion pairs (retention time, m/z , abundance) were imported to SIMCA-P for the model construction.

PCA models were first built to evaluate the similarities among the variables and the robustness of the analytical system. In the PCA scores plots (Figure S1), the pooled QC samples were clustered tightly towards the centre, indicating that satisfactory stability of instrument was achieved. Within each group, none of the samples were analysed as an outlier and no significant differences were observed, further evidencing that the experimental setup was carefully conducted. Clear clustering and separation for different drug treatment and control groups

Next, OPLS-DA models were constructed to identify metabolites with significant changes in abundance between the drug-treated and control groups. In the OPLS-DA scores plots, drug-treated and control groups were clearly clustered and separated, indicating significant distinction of metabolic profiles. However, OPLS-DA is a supervised method with a risk of overfitting the dataset. To evaluate the fitness of model, cross validation and permutation methods (999 times) were further verified. The cross-validation results of OPLS-DA models are summarised in Table S1. The R^2Y and Q^2 value of 0.50 is recommended for cross validation where the model is regarded as accurate⁴¹. The results of cross validation in this study were excellent as the value of R^2Y and Q^2 in each model was ≥ 0.90 . Permutation testing for each OPLS-DA model met the SIMCA-P validity criteria: the original R^2Y and Q^2 values were higher than

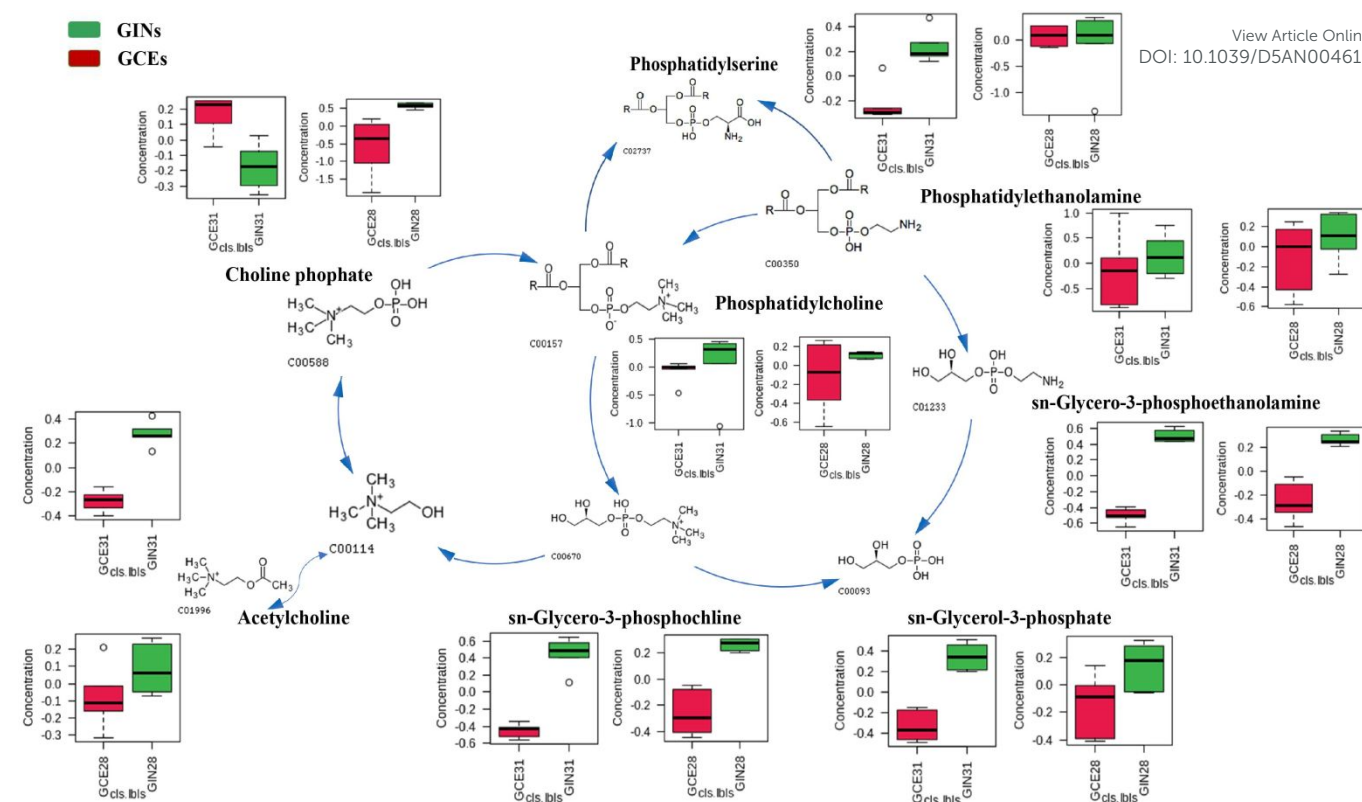


Fig 3. The glycerophospholipid metabolism pathway and the abundance of metabolites identified in GINs and GCEs. The normalised abundance of PC, PE, PS and their metabolites are shown with GCE cells in red and GIN cells in green. The abundance of metabolites was exported from MetaboAnalyst 5.0 and reflects scaled data for visualisation.

all permuted models, the Q^2 regression line had a negative intercept, and the R^2Y and Q^2 regression lines decreased from the original to the permuted models, confirming that the models were not overfitted. Combined with cross validation and permutation results, the models constructed in this study were less likely to overfit our dataset, with good fitness and good predictive ability. Lastly, lists of variables importance in projection (VIP) based on the OPLS-DA models were generated for each comparison. VIP values generally represent the importance of each variable in the OPLS-DA model and have been used to extract the metabolites related to separation. In addition, adjusted p value <0.05 generated from the univariate analysis was combined to select significantly altered metabolites. Hence, in this study, the metabolites with VIP >1 and adjusted p value <0.05 were considered as significantly altered compounds.

Metabolic variation across untreated GBM cells from distinct intra-tumour regions

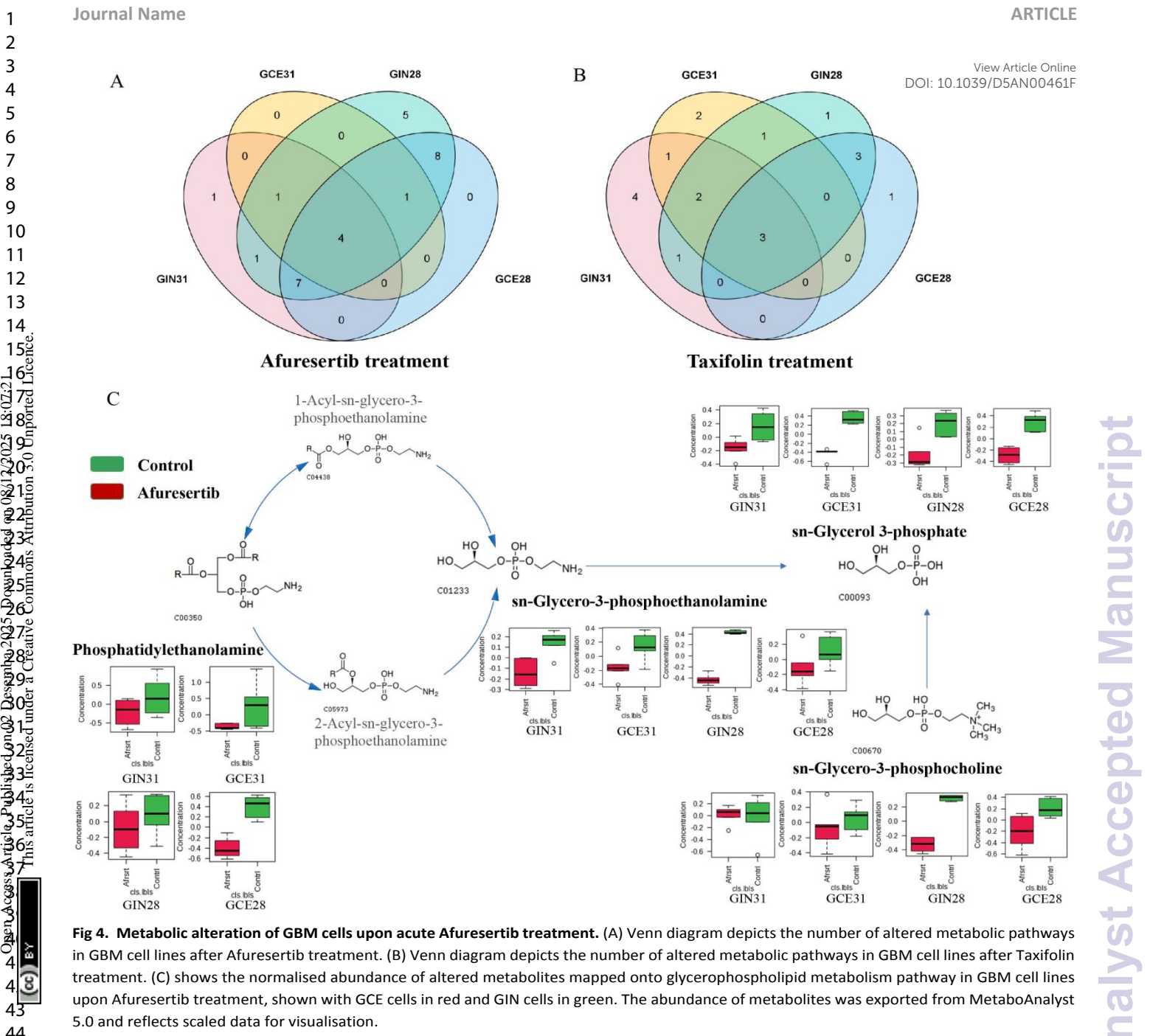
As determined by the PCA scores plots, the cells derived from invasive margin (GINs) and the cells derived from tumor core (GCEs) have been clearly separated. Plots indicated that there were some metabolic differences between respective GINs and GCEs, despite being derived from the same patient tumour. Volcano plots were next used to visually select significantly altered metabolites by combining the statistical p value and fold change (FC) between two groups. The volcano plots of

GIN31/GCE31 and GIN28/GCE28 are shown in Figure S2, where metabolites with FC >2 and adjusted p value <0.05 are highlighted. The number of identified metabolites abundant in GIN31 is greater than that identified in GCE31. However, the number of identified metabolites abundant in GIN28 is less than that identified in GCE28. The results of univariate analysis therefore suggest that intra-tumour metabolic heterogeneity is evident within each patient-derived cell line.

Using well-constructed OPLS-DA models (Figure 2A and 2B), cells from the invasive margin and tumour core were clearly separated, and the significantly altered compounds contributing to this separation are shown in Table S2 and S3.

All the identified metabolites were next submitted to MetaboAnalyst v5.0 for pathway analysis. Pathway analysis performs a vital function in interpreting high dimensional molecular datasets⁴². In MetaboAnalyst v5.0, pathway analysis consists of network analysis and pathway topology analysis. Such networks are a powerful tool for the representation of metabolic pathways. Pathway topology analysis not only lists the components of pathways, but also describes their interaction⁴³. Based on the existing knowledge of biological pathways, metabolites are expected to be mapped onto pathway sets, representing how these metabolites collectively function and interact in biological (healthy and diseased) contexts.

The analysis revealed biochemical signaling and biological processes that are most significantly altered between each



untreated cell line, enriching our understanding of the intrinsic metabolomic profiles of GBM cells propagated *in vitro*. The results of pathway analysis for GIN31/GCE31 are shown in Figure 2C. A total of 58 metabolic pathways were initially identified, which were then filtered to 23 significant metabolic pathways with adjusted *p* value <0.05 and impact factor >0.1 (shown in Table S4). Among these 23 metabolic pathways, most metabolites were related to amino acid metabolism, and where glycerophospholipids/sphingolipids metabolism were more abundant in GIN31. Only metabolites mapped to taurine and hypotaurine metabolism were more abundant in GCE31. Hence, compared to GCE31, GIN31 cells had more active metabolic pathways which were associated with higher demand in energy production, amino acid biosynthesis and phospholipids biosynthesis. The pathway analysis results for untreated GIN28/GCE28 are shown in Table S5. In contrast to GIN31/GCE31, GCE28 cells are more metabolically active than GIN28 cells, with metabolites mapping to pathways including lysine degradation, alanine, aspartate and glutamate metabolism, nicotinate and nicotinamide metabolism, arginine and proline metabolism, glycine, serine and threonine metabolism. Collectively, the results of pathway analysis were consistent with results of univariate analysis presented previously in the volcano plots, indicating the heterogeneity existing between and within patient-derived GBM cell lines.

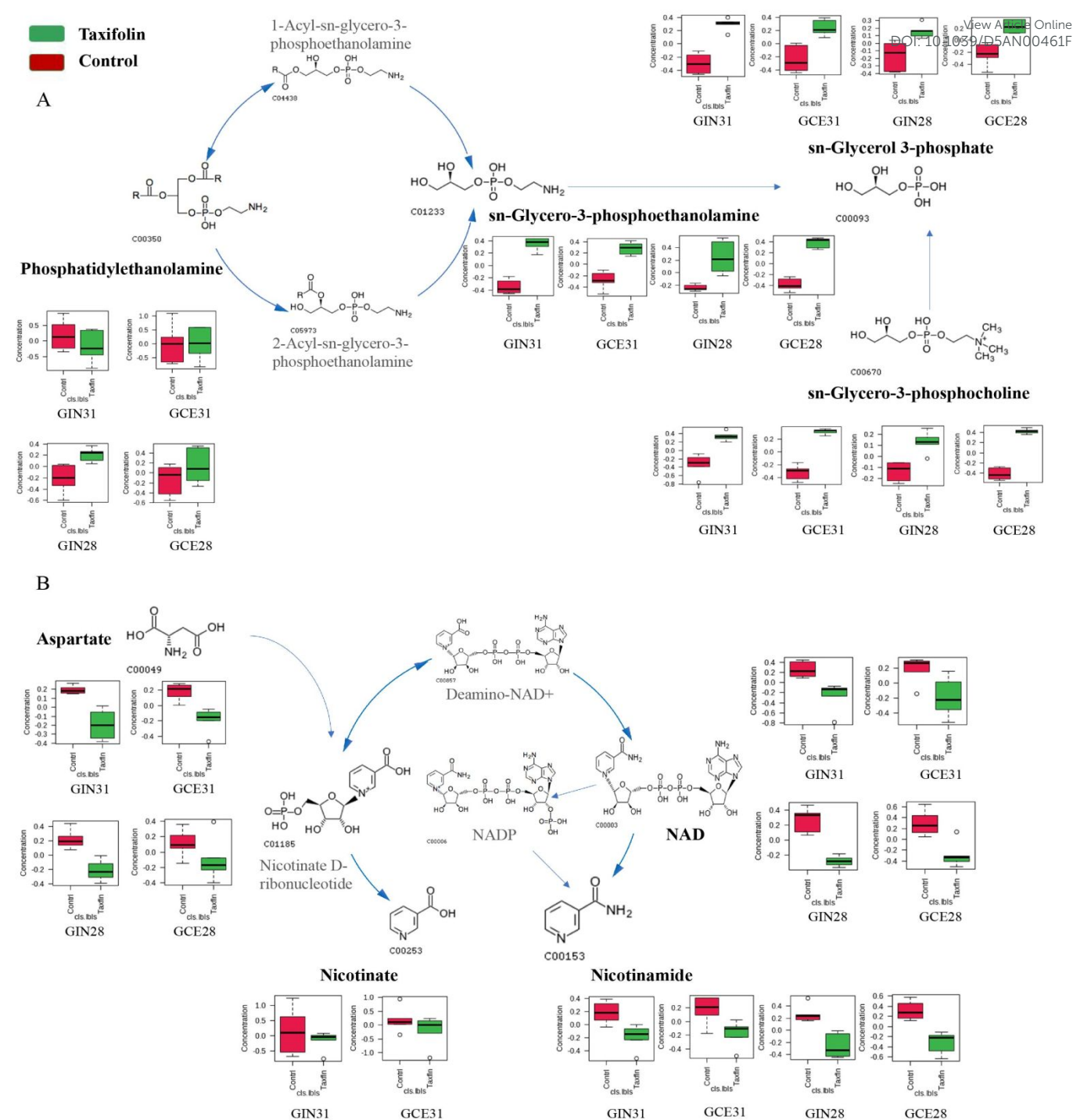


Fig 5. Metabolic pathways altered by Taxifolin treatment. (A) presents the abundance of metabolites related to glycerophospholipid metabolism after Taxifolin treatment. (B) displays the abundance of metabolites mapped onto the nicotinate and nicotinamide metabolism after Taxifolin treatment. The normalised abundance of identified metabolites are shown with untreated cells in red and Taxifolin-treated cells in green. The abundance of metabolites was exported from MetaboAnalyst 5.0 and reflects scaled data for visualisation.

Despite the observed differences existing between cell lines derived from two patients, shown in Figure 2D, 12 shared significant pathways were identified in both GIN31/GCE31 and GIN28/GCE28, including alanine, aspartate and glutamate metabolism, glycerolipid metabolism, glycerophospholipid metabolism, glyoxylate and dicarboxylate metabolism, serine and threonine metabolism, lysine degradation, amino sugar and

nucleotide sugar metabolism, sphingolipid metabolism, cysteine and methionine metabolism, glycine, serine and threonine metabolism, arginine and proline metabolism, and pentose and glucuronate interconversions. Even though the major metabolic pattern of GINs and GCEs was distinct, metabolites which mapped to glycerophospholipid metabolism showed a similar trend. These metabolites included

phosphatidyl choline (PC), phosphatidyl ethanolamine (PE), and phosphatidyl serine (PS), which all exhibited higher abundance in GINs, except for choline phosphate, shown in Figure 3. Additionally, other metabolites which were mapped onto glycerolipid metabolism and sphingolipid metabolism, were more abundant in GIN cells, including serine, sphinganine, and sn-glycerol 3-phosphate.

Changes in glycerophospholipids and their metabolites are closely related to cell membrane fluidity, adhesion, apoptosis, proliferation, invasion, metastasis, angiogenesis, and lymphoangiogenesis^{44, 45}. In cancer cells, increased PC synthesis affects cellular proliferation and programmed cell death⁴⁶. Moreover, the larger amount of PS and PE exposed on the surface of GBM cell membranes compared with healthy cells, increases the negative charges on the outer surface of membranes, inducing mutual repulsion and promoting tumour cell migration^{45, 47}. Collectively, the high abundance of PC, PE, PS and their metabolites could be associated with GINs being derived from infiltrative margin of tumour tissue, indicating their potential as putative metabolic biomarkers for discriminating GINs and GCEs.

Furthermore, phosphatidylinositols are another type of glycerophospholipids which are important mediators of several signalling pathways⁴⁸. It has been reported that the 1-phosphatidyl-1D-myo-inositol-4-phosphate metabolic pathway is related to cell metastasis⁴⁹. Its downstream metabolite, myo-inositol, was identified at higher abundance in GIN28 compared with GCE28, although not detectable in either GIN31 or GCE31, further indicating that this pathway may contribute to the differential metastatic potential observed between GINs and GCEs.

The metabolic pathways altered in GIN/GCE cells upon Afuresertib treatment

To investigate metabolic pathways affected by drug treatment, the results of pathway analysis and selected significant pathways for each cell line after Afuresertib treatment are summarised in Table S6-S9.

As shown in Figure 4A, compared with the untreated group, 14 significant pathways were identified in GIN31 after Afuresertib treatment, and 6 metabolic pathways were identified for GCE31. The pathways identified in GIN31 and GCE31 showed high similarity as 5 pathways were shared in both cell lines. A similar phenomenon was observed in GIN28 and GCE28, indicating that Afuresertib might exert a similar downstream effect in cells derived from different tumour locations from the same patient. Four metabolic pathways were identified which were shared by all four GBM cell lines upon Afuresertib exposure, including alanine, aspartate and glutamate metabolism, histidine metabolism, cysteine and methionine metabolism, and glycerophospholipid metabolism.

Afuresertib treatment broadly suppressed amino acid metabolism in GBM cells. The level of alanine, which replenishes the nutrient sink for rapidly proliferating GBM cells⁵⁰, was decreased. The glutamate and glutamine cycle, typically upregulated to meet the requirement for biosynthesis of proteins, lipids, and nucleic acids⁵¹, was also disrupted. Their

abundance was decreased, along with aspartate, a downstream product of glutamine oxidation, crucial for protein and nucleotide biosynthesis⁵². Exogenous methionine, essential for GBM colony formation and survival *in vitro*⁵³, showed reduced abundance. The level of other amino acids, including phenylalanine and tryptophan, were decreased in some GBM cells received treatment, although they were not identified as major altered pathways. Collectively, these reductions indicate that Afuresertib exerts its anti-tumour activity by limiting the availability of amino acids necessary for tumour survival and progression.

In addition, the abundance of metabolites involved in glycerophospholipid metabolism were lower in Afuresertib-treated cells (Figure 4C). Given that alterations in glycerophospholipid metabolism can affect cell membrane composition, fluidity, and downstream signalling, Afuresertib may also induce cell death by disrupting membrane integrity and impairing signalling pathways.

The metabolic pathways altered in GIN/GCE cells upon Taxifolin treatment

Identified significant pathways for each cell line upon Taxifolin treatment are summarised in Table S6-S9. As shown in Figure 4B, only 3 pathways were shared for all tested GBM cell lines after Taxifolin exposure (histidine metabolism, nicotinate and nicotinamide metabolism and glycerophospholipid metabolism).

Compared to untreated cells, Taxifolin treatment resulted in reduced levels of several metabolites involved in histidine metabolism, including histidine, histamine, aspartate, and glutamate. Apart from that, the abundance of metabolites associated with nicotinate and nicotinamide metabolism were also decreased (Figure 5B). Nicotinamide adenine dinucleotide (NAD⁺) and its degradation products are key regulators of glycolysis, oxidative phosphorylation and tricarboxylic acid (TCA) cycle⁵⁴. Our results indicated that Taxifolin may interfere with cellular energy metabolism by lowering these critical metabolites. Moreover, NAD⁺ acts as a substrate for multiple downstream signalling pathways, including DNA repairment, post-translational modification, inflammatory response, and apoptosis⁵⁵. The observed reduction suggested that Taxifolin may further disrupt these processes, associated with impaired metabolic activity.

Glycerophospholipid metabolism was also identified as a significant pathway in GBM cells exposed to Taxifolin. In contrast to Afuresertib treatment, the abundance of metabolites in this pathway were identified at a higher level in treated cells (Figure 5A). The results indicated that Taxifolin may not inhibit glycerophospholipid metabolism.

Distinct metabolic pattern between untreated GBM cells and astrocytes

To understand whether these identified metabolic pathways affected by Afuresertib and Taxifolin are specifically relative to GBM disease, experiments were repeated to compare the metabolic difference between GBM cells and astrocytes. The



ARTICLE

Journal Name

GBM cell lines were first successfully adapted to astrocyte medium.

The astrocytes and GBM cells were clearly separated in the scores plot of both PCA and OPLS-DA (shown in Figure S3, S4 and Table S10), indicating the distinct metabolic differences existing among groups. As shown in Figure S5, six metabolic pathways (adjusted p value <0.05 and impact factor >0.1) were shared across the comparisons of astrocytes vs. GBM cells: alanine, aspartate and glutamate metabolism, sphingolipid metabolism, glutathione metabolism, glycerophospholipid metabolism, TCA cycle, and taurine and hypotaurine metabolism.

As shown in Figure S6, the abundance of metabolites mapped onto glycerophospholipid metabolism were at higher levels in GBM cells, indicating that this pathway is more active in GBM cells relative to astrocytes. The level of hypotaurine was also higher in GBM cells relative to astrocytes, consistent with studies which reported that hypotaurine in tumour tissue was significantly higher than that in adjacent control tissue^{56, 57}. In addition, a higher level of glutathione was observed in GBM cells. It has been reported that increased glutathione has a positive association with chemo-resistance in GBM⁵⁸⁻⁶⁰.

The metabolic differences between GINs and GCEs were also observed when cells were cultured in astrocyte medium. As determined by the volcano plots (Figure S7) and pathway analysis, the data showed a similar trend with that generated from DMEM medium, providing supportive evidence that adapting GBM cells into astrocytes medium did not change the metabolic pattern between GBM cells.

Metabolic pathways altered in astrocytes upon drug treatment

Although no selectivity of either Afuresertib or Taxifolin was observed between GBM cells and astrocytes based on the metabolic viability results, drug treatment in astrocytes was still valuable to assess significant changes in metabolites and metabolic pathways, comparing these effects with those observed in GBM cells. This approach aimed to further explore whether the previously identified pathways affected by the two drugs were specifically associated with anti-tumour functions. The control and drug treatment groups were clearly separated in PCA and OPLS-DA scores plots (Figure S8), indicating distinct metabolic differences between untreated and treated astrocytes.

As previously mentioned, after Afuresertib treatment, four metabolic pathways were commonly affected across all GBM cell lines. Of these, three pathways, (alanine, aspartate and glutamate metabolism, histidine metabolism, and glycerophospholipid metabolism), were also altered in astrocytes. Similarly, the three pathways affected in GBM cells following Taxifolin exposure were also identified in astrocytes received Taxifolin treatment.

Metabolites (except for aspartate) involved in nicotinate and nicotinamide metabolism showed lower abundance in Taxifolin-treated group compared to controls. Additionally, metabolites mapped onto glycerophospholipid metabolism displayed lower abundance in Afuresertib-treated group while

higher abundance in Taxifolin-treated group, compared with controls (Figure S9).

DOI: 10.1039/D5AN00461F

These findings suggest that the metabolic pathways altered by these drugs were not tumour specific as drug-induced metabolic responses in astrocytes were consistent with those observed in GBM cells. Additionally, the consistent drug response observed in both GBM cells and astrocytes supported the proposed mechanism of action from a metabolomics perspective.

Invasion assay

As discussed previously, changes in glycerophospholipids and their metabolites are closely related to cell membrane fluidity, adhesion and invasion. Based on the results of metabolomics study, the metabolites involved in glycerophospholipid metabolism were at lower abundance upon Afuresertib treatment but not upon Taxifolin treatment. Hence, we next investigated the ability of Afuresertib and Taxifolin to inhibit cell invasion.

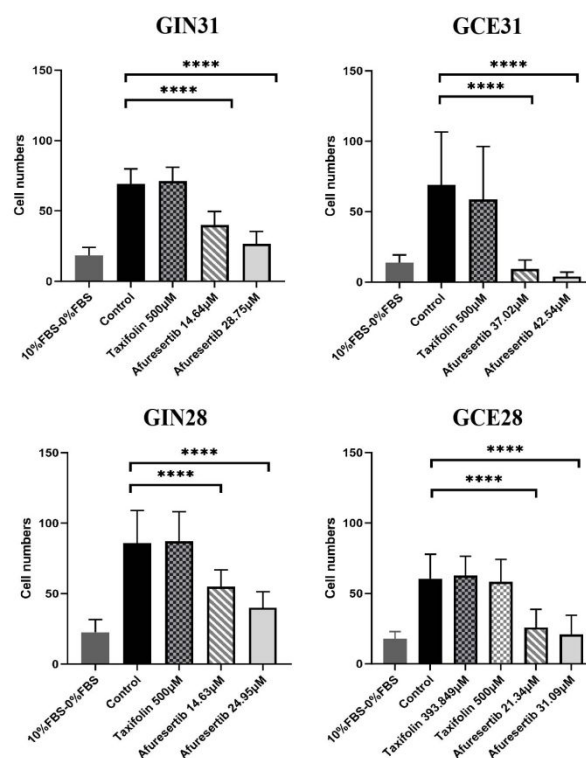


Fig 6. Assessment of putative anti-invasion effects on GBM cells upon Afuresertib and Taxifolin treatment. The Transwell collagen-barrier assay was adopted to investigate the anti-invasion ability of repurposed candidates on four GBM cell lines. The two concentrations of Afuresertib (IC_{25} and IC_{50}) were tested on four cell lines, while only 500 μ M Taxifolin was tested on GBM cells, except for GCE28. The invaded cells were fixed before being stained by 0.2% crystal violet. Images from four different fields of view were taken under a light microscope (10X) and the number of invaded cells were counted.

The results are presented in Figure 6 and S10. Considering the comparison of the number of invaded cells between control and drug-treated groups, Afuresertib significantly inhibited the ability of GBM cells invading through the collagen barrier in a concentration-dependent manner. No statistical difference was observed between the Taxifolin treated and control groups

1
2
3
4
5
6
7
8
9
10
11
12
13
14
15
16
17
18
19
20
21
22
23
24
25
26
27
28
29
30
31
32
33
34
35
36
37
38
39
40
41
42
43
44
45
46
47
48
49
50
51
52
53
54
55
56
57
58
59
60

across all cell lines, indicating that Taxifolin did not inhibit the GBM cell invasion within this experimental context.

Discussion

In order to develop an effective therapeutic for GBM, its pharmacokinetic profile, molecular mechanism, and safety need to be fully investigated. Clinically, single-agent Afuresertib showed a favourable pharmacokinetic and safety profile, with a maximum tolerated dose of 125 mg/day⁶¹. However, its ability to penetrate the blood-brain barrier has not been reported, raising uncertainty about its therapeutic potential in brain tumours *in vivo*. The safety of Taxifolin has been well studied and toxic effects from overdose have not been reported, including mutagenicity, embryotoxicity and immunotoxicity⁶². Taxifolin was detectable in rat brain⁶³. However, its low bioavailability (approximately 0.17%) presents a main limitation for clinical use⁶⁴. Hence, given our *in vitro* findings, clear molecular mechanism, and reported clinical safety, Afuresertib is a promising anti-GBM candidate.

Based on the results of the viability tests, GINs were more sensitive to Afuresertib than GCEs, and the mechanism underlying this difference is unknown. Given that Afuresertib is an AKT inhibitor, to explore this further, the difference in AKT gene expression was measured between GINs and GCEs. The results showed that the heterogeneity of GBM was evident at the genetic level (Figure S11). Although the qPCR results did not directly explain the differences in sensitivity, they underscore the complexity of gene regulation, as gene expression does not necessarily correlate with protein levels. Further investigation of AKT protein expression combined with gene expression may better elucidate these mechanisms.

Although *in vitro* metabolic viability and metabolomics results showed no selectivity of drugs between tumour and healthy cells, further investigation is still worth. Since laboratory-cultured astrocytes are required to be in a progenitor state (to permit propagation), this does not reflect the majority of astrocytes in the GBM tumour microenvironment, which are terminally differentiated (post-mitotic) mature cells, and therefore likely to be less sensitive to intracellular drug uptake⁶⁵.

This suggests that clinically there may be a therapeutic window which has not been replicated *in vitro*. Therefore, the predominance of post-mitotic astrocytes in a patient-derived rodent xenograft model will be a more accurate to determine a tolerated dose and a potential therapeutic window.

This study revealed intra-tumour metabolic heterogeneity in GBM at the cellular level. In our previous work on metabolic heterogeneity in IDH wild-type GBM primary tissue, it was found regional heterogeneity in glycolysis, TCA cycle and energy-related metabolites. For example, invasive regions were rich in D-glucose and citrate, while non-invasive areas showed higher levels of ATP and NADH⁶⁶. These patterns were not observed in the current study, likely due to differences in patient samples and the use of cell lines rather than primary tumour tissue.

Glycerophospholipid metabolism was identified as more active in GINs relative to GCEs, indicating potential variability in underlying genetic or epigenetic mutations within GINs and GCEs. From the perspective of metabolomics, our results add to the knowledge base and rationale supportive of deriving GBM cell lines from different regions. Upon drug treatment, glycerophospholipid metabolism was also identified as a significantly altered pathway in GBM cells. Combined with the results from invasion assay, we hypothesise that Afuresertib impairs invasion *in vitro* by perturbing glycerophospholipid metabolism. To test this hypothesis directly, metabolites should be extracted from drug-treated cells within the Transwell invasion chamber and subjected to metabolomic profiling.

Conclusions

This study evaluated the potential of repurposed Afuresertib and Taxifolin for GBM treatment *in vitro* and revealed their potential anti-tumour metabolic mechanisms. Observed anti-tumour phenotypes upon drug exposure provide evidence that these compounds are sufficient to induce these phenotypes *in vitro*, despite being agnostic to whether they are necessary *in vivo*. Further assessment of drug efficacy in GBM xenograft models will be required to validate these findings.

We cannot conclude that our *in vitro* findings fully represent GBM tumour tissue, unless metabolic changes are associated with underlying genetic or epigenetic mutations which are maintained with high fidelity in culture conditions. Our data does not determine what proportion of observed metabolic profiles in untreated GBM cells are related to *in vitro* propagation and which are representative of *in situ* tumour metabolism. Future work will need to cross-validate these *in vitro* profiles against primary tumour infiltrative margin tissue. Nevertheless, observed anti-tumour phenotypes upon Afuresertib and Taxifolin exposure provide evidence that these drug compounds are sufficient to induce these phenotypes *in vitro*, despite being agnostic to whether they are necessary *in vivo*. Further studies to assess drug efficacy in GBM orthotopic xenograft models will be required to validate these findings.

Author Contributions

R.C: investigation, methodology, data analysis, manuscript writing; N.G: support for cell culture, sample preparation, manuscript reviewing; S.J: support for qPCR analysis, sample preparation, manuscript reviewing; A.W: support for sample acquisition and data analysis, manuscript reviewing; R.R and D-H. K: supervision, project management, conceptualisation, draft editing and revised.

Conflicts of interest

There are no conflicts to declare.

Acknowledgements

Analyst Accepted Manuscript

This work was supported by the University of Nottingham Centre for Analytical Bioscience (School of Pharmacy), and Children's Brain Tumour Research Centre (School of Medicine).

References

1. M. Weller, M. van den Bent, M. Preusser, E. Le Rhun, J. C. Tonn, G. Minniti, M. Bendszus, C. Balana, O. Chinot, L. Dirven, P. French, M. E. Hegi, A. S. Jakola, M. Platten, P. Roth, R. Ruda, S. Short, M. Smits, M. J. B. Taphoorn, A. von Deimling, M. Westphal, R. Soffietti, G. Reifenberger and W. Wick, *Nat Rev Clin Oncol*, 2022, **19**, 357-358.
2. A. Hatoum, R. Mohammed and O. Zakieh, *Cancer Manag Res*, 2019, **11**, 1843-1855.
3. S. Jiapaer, T. Furuta, S. Tanaka, T. Kitabayashi and M. Nakada, *Neurol Med Chir (Tokyo)*, 2018, **58**, 405-421.
4. R. Liu, X. P. Qin, Y. Zhuang, Y. Zhang, H. B. Liao, J. C. Tang, M. X. Pan, F. F. Zeng, Y. Lei, R. X. Lei, S. Wang, A. C. Liu, J. Chen, Z. F. Zhang, D. Zhao, S. L. Wu, R. Z. Liu, Z. F. Wang and Q. Wan, *Cancer Med*, 2018, **7**, 2848-2859.
5. C. B. Crivii, A. B. Bosca, C. S. Melincovici, A. M. Constantin, M. Marginean, E. Dronca, R. Sufletel, D. Gonciar, M. Bungardean and A. Sovrea, *Cancers (Basel)*, 2022, **14**.
6. J. L. Izquierdo-Garcia, P. Viswanath, P. Eriksson, M. M. Chaumeil, R. O. Pieper, J. J. Phillips and S. M. Ronen, *PLoS One*, 2015, **10**, e0118781.
7. T. T. Lah, M. Novak and B. Breznik, *Semin Cancer Biol*, 2020, **60**, 262-273.
8. K. Jaroch, P. Modrakowska and B. Bojko, *Metabolites*, 2021, **11**.
9. A. A. Mohan, W. H. Tomaszewski, A. P. Haskell-Mendoza, K. M. Hotchkiss, K. Singh, J. L. Reedy, P. E. Fecci, J. H. Sampson and M. Khasraw, *Front Oncol*, 2021, **11**, 696402.
10. C. Lu, P. S. Ward, G. S. Kapoor, D. Rohle, S. Turcan, O. Abdel-Wahab, C. R. Edwards, R. Khanin, M. E. Figueroa, A. Melnick, K. E. Wellen, D. M. O'Rourke, S. L. Berger, T. A. Chan, R. L. Levine, I. K. Mellinghoff and C. B. Thompson, *Nature*, 2012, **483**, 474-478.
11. P. Chinnaiyan, E. Kensicki, G. Bloom, A. Prabhu, B. Sarcar, S. Kahali, S. Eschrich, X. Qu, P. Forsyth and R. Gillies, *Cancer Res*, 2012, **72**, 5878-5888.
12. L. B. Wang, A. Karpova, M. A. Gritsenko, J. E. Kyle, S. Cao, Y. Li, D. Rykunov, A. Colaprico, J. H. Rothstein, R. Hong, V. Stathias, M. Cornwell, F. Petralia, Y. Wu, B. Reva, K. Krug, P. Pugliese, E. Kawaler, L. K. Olsen, W. W. Liang, X. Song, Y. Dou, M. C. Wendl, W. Caravan, W. Liu, D. Cui Zhou, J. Ji, C. F. Tsai, V. A. Petyuk, J. Moon, W. Ma, R. K. Chu, K. K. Weitz, R. J. Moore, M. E. Monroe, R. Zhao, X. Yang, S. Yoo, A. Krek, A. Demopoulos, H. Zhu, M. A. Wyczalkowski, J. F. McMichael, B. L. Henderson, C. M. Lindgren, H. Boekweg, S. Lu, J. Baral, L. Yao, K. G. Stratton, L. M. Bramer, E. Zink, S. P. Couvillion, K. J. Bloodsworth, S. Satpathy, W. Sieh, S. M. Boca, S. Schurer, F. Chen, M. Wiznerowicz, K. A. Ketchum, E. S. Boja, C. R. Kinsinger, A. I. Robles, T. Hiltke, M. Thiagarajan, A. I. Nesvizhskii, B. Zhang, D. R. Mani, M. Ceccarelli, X. S. Chen, S. L. Cottingham, Q. K. Li, A. H. Kim, D. Fenyó, K. V. Ruggles, H. Rodriguez, M. Mesri, S. H. Payne, A. C. Resnick, P. Wang, R. D. Smith, A. Iavarone, M. G. Chheda, J. S. Barnholtz-Sloan, K. D. Rodland, T. Liu, L. Ding and C. Clinical Proteomic Tumor Analysis, *Cancer Cell*, 2021, **39**, 509-528 e520. DOI: 10.1039/D5AN00461F
13. U. D. Kahlert, K. Koch, A. K. Suwala, R. Hartmann, M. Cheng, D. Maciaczyk, D. Willbold, C. G. Eberhart, K. Glunde and J. Maciaczyk, *Folia Neuropathol*, 2015, **53**, 219-225.
14. R. Zhang, P. S. Hu, Q. C. Zang, X. F. Yue, Z. Zhou, X. Y. Xu, J. Xu, S. S. Li, Y. H. Chen, B. Q. Qiang, X. Z. Peng, W. Han, R. P. Zhang and Z. Abliz, *Rsc Adv*, 2017, **7**, 24221-24232.
15. S. L. Perrin, M. S. Samuel, B. Koszyca, M. P. Brown, L. M. Ebert, M. Oksdath and G. A. Gomez, *Biochem Soc Trans*, 2019, **47**, 625-638.
16. R. Liu, L. Wei and P. Zhang, *Nat Mach Intell*, 2021, **3**, 68-75.
17. K. D. Rutherford, G. K. Mazandu and N. J. Mulder, *Brief Funct Genomics*, 2018, **17**, 34-41.
18. S. Pushpakom, F. Iorio, P. A. Eyers, K. J. Escott, S. Hopper, A. Wells, A. Doig, T. Williams, J. Latimer, C. McNamee, A. Norris, P. Sanseau, D. Cavalla and M. Pirmohamed, *Nat Rev Drug Discov*, 2019, **18**, 41-58.
19. C. S. Greene and B. F. Voight, *Hum Mol Genet*, 2016, **25**, R94-R98.
20. C. Tomi-Andrino, A. Pandele, K. Winzer, J. King, R. Rahman and D. H. Kim, *Sci Rep*, 2022, **12**, 11189.
21. F. B. Furnari, T. F. Cloughesy, W. K. Cavenee and P. S. Mischel, *Nat Rev Cancer*, 2015, **15**, 302-310.
22. A. Barzegar Behrooz, Z. Talaie, F. Jusheghani, M. J. Los, T. Klönisch and S. Ghavami, *Int J Mol Sci*, 2022, **23**.
23. M. Hutt-Cabezaz, M. A. Karajannis, D. Zagzag, S. Shah, I. Horkayne-Szakaly, E. J. Rushing, J. D. Cameron, D. Jain, C. G. Eberhart, E. H. Raabe and F. J. Rodriguez, *Neuro Oncol*, 2013, **15**, 1604-1614.
24. N. E. Uko, O. F. Guner, D. F. Matesic and J. P. Bowen, *Curr Top Med Chem*, 2020, **20**, 883-900.
25. S. P. Blagden, A. L. Hamilton, L. Mileshekin, S. Wong, A. Michael, M. Hall, J. C. Goh, A. S. Lisyanskaya, M. DeSilvio, E. Frangou, E. A. Stronach, P. Gopalakrishna, T. M. Meniawy and H. Gabra, *Clin Cancer Res*, 2019, **25**, 1472-1478.
26. C. I. Chen, H. Paul, L. W. Le, E. N. Wei, S. Snitzler, T. Wang, O. Levina, S. Kakar, A. Lau, M. Queau, J. B. Johnston, D. A. Smith and S. Trudel, *Leuk Lymphoma*, 2019, **60**, 92-100.
27. J. Wang, X. Xu, T. Wang, Q. Guo, X. Dai, H. Guo, W. Zhang, S. Cheng, X. Chen and L. Ding, *Eur J Pharmacol*, 2021, **896**, 173879.
28. B. Min, Y. Wang, F. Liang, C. X. Wang, F. Wang and Z. Yang, *Dis Markers*, 2022, **2022**, 1832241.
29. Y. Zu, W. Wu, X. Zhao, Y. Li, W. Wang, C. Zhong, Y. Zhang and X. Zhao, *Int J Pharm*, 2014, **471**, 366-376.
30. Z. Hu, L. Xuan, T. Wu, N. Jiang, X. Liu, J. Chang, T. Wang, N. Han and X. Tian, *Int Immunopharmacol*, 2023, **114**, 109616.
31. R. Yang, X. Yang and F. Zhang, *Curr Neuropharmacol*, 2023, DOI: 10.2174/1570159X21666230203101107.
32. W. Q. Yao, H. Y. Gong, H. Mei, L. Shi, J. M. Yu and Y. Hu, *J Oncol*, 2021, **2021**.
33. C. R. Justus, M. A. Marie, E. J. Sanderlin and L. V. Yang, *Methods Mol Biol*, 2023, **2644**, 349-359.
34. D. S. Wishart, A. Guo, E. Oler, F. Wang, A. Anjum, H. Peters, R. Dizon, Z. Sayeeda, S. Tian, B. L. Lee, M. Berjanskii, R. Mah, M. Yamamoto, J. Jovel, C. Torres-Calzada, M. Hiebert-Giesbrecht, V. W. Lui, D. Varshavi, D. Varshavi, D. Allen, D. Arndt, N. Khetarpal, A. Sivakumaran, K. Harford, S. Sanford, K. Yee, X. Cao, Z. Budinski, J. Liigand, L. Zhang, J. Zheng, R.

- Mandal, N. Karu, M. Dambrova, H. B. Schioth, R. Greiner and V. Gautam, *Nucleic Acids Res*, 2022, **50**, D622-D631.
35. L. W. Sumner, A. Amberg, D. Barrett, M. H. Beale, R. Beger, C. A. Daykin, T. W. Fan, O. Fiehn, R. Goodacre, J. L. Griffin, T. Hankemeier, N. Hardy, J. Harnly, R. Higashi, J. Kopka, A. N. Lane, J. C. Lindon, P. Marriott, A. W. Nicholls, M. D. Reilly, J. J. Thaden and M. R. Viant, *Metabolomics*, 2007, **3**, 211-221.
36. L. W. Sumner, Z. Lei, B. J. Nikolau, K. Saito, U. Roessner and R. Trengove, *Metabolomics*, 2014, **10**, 1047-1049.
37. Z. Pang, G. Zhou, J. Ewald, L. Chang, O. Hacariz, N. Basu and J. Xia, *Nat Protoc*, 2022, **17**, 1735-1761.
38. M. Xu, D. J. McCanna and J. G. Sivak, *J Pharmacol Toxicol Methods*, 2015, **71**, 1-7.
39. B. Luzak, P. Siarkiewicz and M. Boncler, *Toxicol In Vitro*, 2022, **83**, 105407.
40. A. M. Evans, C. O'Donovan, M. Playdon, C. Beecher, R. D. Beger, J. A. Bowden, D. Broadhurst, C. B. Clish, S. Dasari, W. B. Dunn, J. L. Griffin, T. Hartung, P. C. Hsu, T. Huan, J. Jans, C. M. Jones, M. Kachman, A. Kleensang, M. R. Lewis, M. E. Monge, J. D. Mosley, E. Taylor, F. Tayyari, G. Theodoridis, F. Torta, B. K. Ubhi, D. Vuckovic and Q. C. C. Metabolomics Quality Assurance, *Metabolomics*, 2020, **16**, 113.
41. R. Shaffer, *Journal of Chemometrics - J CHEMOMETR*, 2002, **16**, 261-262.
42. C. Wieder, C. Frainay, N. Poupin, P. Rodriguez-Mier, F. Vinson, J. Cooke, R. P. Lai, J. G. Bundy, F. Jourdan and T. Ebbels, *PLoS Comput Biol*, 2021, **17**, e1009105.
43. M. A. Garcia-Campos, J. Espinal-Enriquez and E. Hernandez-Lemus, *Front Physiol*, 2015, **6**, 383.
44. Y. Xu, B. Dong, J. Wang, J. Zhang, W. Xue and Y. Huang, *Oncoimmunology*, 2018, **7**, e1502130.
45. S. Riedl, B. Rinner, M. Asslaber, H. Schaidler, S. Walzer, A. Novak, K. Lohner and D. Zwegitck, *Biochim Biophys Acta*, 2011, **1808**, 2638-2645.
46. N. D. Ridgway, *Crit Rev Biochem Mol Biol*, 2013, **48**, 20-38.
47. H. Zhou, J. H. Stafford, R. R. Hallac, L. Zhang, G. Huang, R. P. Mason, J. Gao, P. E. Thorpe and D. Zhao, *J Biomed Nanotechnol*, 2014, **10**, 846-855.
48. S. Furse, N. J. Brooks, A. M. Seddon, R. Woscholski, R. H. Templer, E. W. Tate, P. R. Gaffney and O. Ces, *Soft Matter*, 2012, **8**, 3090-3093.
49. D. Rajamanoharan, H. V. McCue, R. D. Burgoyne and L. P. Haynes, *Mol Biol Cell*, 2015, **26**, 1428-1439.
50. S. Firdous, R. Abid, Z. Nawaz, F. Bukhari, A. Anwer, L. L. Cheng and S. Sadaf, *Metabolites*, 2021, **11**.
51. S. Venneti and C. B. Thompson, *Annu Rev Pathol*, 2017, **12**, 515-545.
52. R. Gorgoglione, V. Impedovo, C. L. Riley, D. Fratantonio, S. Tiziani, L. Palmieri, V. Dolce and G. Fiermonte, *Cancers (Basel)*, 2022, **14**.
53. K. Palanichamy, K. Thirumoorthy, S. Kanji, N. Gordon, R. Singh, J. R. Jacob, N. Sebastian, K. T. Litzenberg, D. Patel, E. Bassett, B. Ramasubramanian, T. Lautenschlaeger, S. M. Fischer, A. Ray-Chaudhury and A. Chakravarti, *Clin Cancer Res*, 2016, **22**, 3513-3523.
54. C. C. S. Chini, J. D. Zeidler, S. Kashyap, G. Warner and E. N. Chini, *Cell Metab*, 2021, **33**, 1076-1087.
55. R. S. Fletcher and G. G. Lavery, *J Mol Endocrinol*, 2018, **61**, R107-R121.
56. P. Gao, C. Yang, C. L. Nesvick, M. J. Feldman, S. Sizdahkhani, H. Liu, H. Chu, F. Yang, L. Tang, J. Tian, S. Zhao, G. Li, J. D. Heiss, Y. Liu, Z. Zhuang and G. Xu, *Oncotarget*, 2016, **7**, 15200-15214. DOI: 10.1039/D5AN00461F
57. D. Shen, L. Tian, F. Yang, J. Li, X. Li, Y. Yao, E. W. Lam, P. Gao, B. Jin and R. Wang, *Cell Death Discov*, 2021, **7**, 21.
58. C. R. Rocha, C. C. Garcia, D. B. Vieira, A. Quinet, L. C. de Andrade-Lima, V. Munford, J. E. Belizario and C. F. Menck, *Cell Death Dis*, 2015, **6**, e1727.
59. R. Tjong, P. Stavrinou, G. Rohn, B. Krischek, A. Koch, R. Goldbrunner and M. Timmer, *Anticancer Res*, 2019, **39**, 1795-1805.
60. Z. Zhu, S. Du, Y. Du, J. Ren, G. Ying and Z. Yan, *J Neurochem*, 2018, **144**, 93-104.
61. A. Spencer, S. S. Yoon, S. J. Harrison, S. R. Morris, D. A. Smith, R. A. Brigandi, J. Gauvin, R. Kumar, J. B. Opalinska and C. Chen, *Blood*, 2014, **124**, 2190-2195.
62. S. V. Orlova, V. V. Tatarinov, E. A. Nikitina, A. V. Sheremeta, V. A. Ivlev, V. G. Vasil'ev, K. V. Paliy and S. V. Goryainov, *Pharm Chem J*, 2022, **55**, 1133-1137.
63. N. Efsa Panel on Dietetic Products, Allergies, D. Turck, J. L. Bresson, B. Burlingame, T. Dean, S. Fairweather-Tait, M. Heinonen, K. I. Hirsch-Ernst, I. Mangelsdorf, H. J. McArdle, A. Naska, M. Neuhauser-Berthold, G. Nowicka, K. Pentieva, Y. Sanz, A. Siani, A. Sjodin, M. Stern, D. Tome, M. Vinceti, P. Willatts, K. H. Engel, R. Marchelli, A. Poting, M. Poulsen, J. Schlatter, W. Gelbmann and H. Van Loveren, *EFSA J*, 2017, **15**, e04682.
64. X. Wang, H. Xia, F. Xing, G. Deng, Q. Shen and S. Zeng, *J Chromatogr B Analyt Technol Biomed Life Sci*, 2009, **877**, 1778-1786.
65. A. Herrero-Navarro, L. Puche-Aroca, V. Moreno-Juan, A. Sempere-Ferrandez, A. Espinosa, R. Susin, L. Torres-Masjoan, E. Leyva-Diaz, M. Karow, M. Figueres-Onate, L. Lopez-Mascaraque, J. P. Lopez-Atalaya, B. Berninger and G. Lopez-Bendito, *Sci Adv*, 2021, **7**.
66. J. Wood, S. J. Smith, M. Castellanos-Urbe, A. Lourdasamy, S. T. May, D. A. Barrett, R. G. Grundy, D. H. Kim and R. Rahman, *Heliyon*, 2025, **11**, e41309.

Data Availability

View Article Online
DOI: 10.1039/D5AN00461F

The original data presented in the study will be openly available after acceptance in the Nottingham Research Data Management Repository at <https://rdmc.nottingham.ac.uk/>

